Journal of Current Science and Technology, January-April 2021 Vol. 11 No. 1, pp. 32-39

ISSN 2630-0656 (Online)

Cite this article: Panyanon, C., Dungkaew, W., & Chainok, K. (2021, January). Synthesis and structural characterization of (Na6F(H2O)18[(VO4)2]•2H3O•2HF. *Journal of Current Science and Technology, 11*(1), 32-39. DOI: 10.14456/jcst.2021.6

Journal of Current Science and Technology

Journal homepage: https://jcst.rsu.ac.th

Synthesis and structural characterization of $(Na_6F(H_2O)_{18}[(VO_4)_2]\cdot 2H_3O\cdot 2HF$

Chana Panyanon[1], Winya Dungkaew[2], and Kittipong Chainok[1]*

[1]Thammasat University Research Unit in Multifunctional Crystalline Materials and Applications (TU-McMa), Faculty of Science and Technology, Thammasat University, Pathumthani 12121, Thailand
[2]Department of Chemistry, Faculty of Science, Mahasarakham University, Mahasarakham 44150, Thailand

*Corresponding author; Email: kc@tu.ac.th

Received 30 August 2020; Revised 25 November 2020; Accepted 3 December 2020;
Published online 30 January 2021

Abstract

A new sodium vanadate solid comprising hexameric Na_6 cluster, $(Na_6F(H_2O)_{18})[(VO_4)_2]\cdot 2H_3O\cdot 2HF$ (**1**), was synthesized for the first time. Material **1** was characterized by single crystal X-ray diffraction (SC-XRD), powder X-ray diffraction (PXRD), infrared spectroscopy (IR), and thermogravimetric analysis (TGA). **1** crystallizes in the cubic system with space group *Fd*-3*c* and the crystal comprises two orthovanadate (VO_4) units, one hexameric sodium $[Na_6F(H_2O)_{18}]$ cluster, two hydrogen fluoride (HF) molecules, and two oxonium (H_3O) cations. In the crystal, the four moieties interact with each other through extensive O−H···O and O−H···F hydrogen bonding interactions to give rise to a three-dimensional supramolecular architecture. The discrete structure of **1** can be transformed to an infinite three-dimensional network of β-$NaVO_3$ phase via thermally induced solid-state reactivity.

Keywords**:** *hexanuclear; hexameric Na_6 cluster; oxonium; single crystal to single crystal transformation; sodium cluster; vanadate.*

1. Introduction

Vanadium oxides have received extensive attention from both the industrial and academic communities due to their rich structural features with a range of physical and chemical properties suitable for applications in catalysis (Wanna et al., 2019), high energy density lithium batteries (Mattelaer et al., 2016), cathode materials for fuel cells (Shanmugam, Ayyaru, & Ahn, 2018), magnetism (Akande et al., 2015), and optical devices (Cong et al., 2010). As a subclass of polyoxometallates (POMs), many compounds based on oxovanadium have significant industrial applications as a catalyst in the manufacturing processes. For instance, magnesium vanadates (MgV_xO_y; x = 1-3, y = 3-8) have been used as selective oxidative catalysts in the production of sulfuric acids and other useful chemicals (Bouloux, Milosevic, & Galy, 1976; Gopal, & Calvo, 1974; Millet, Satto, Sciau, & Galy, 1998). Calcium vanadate ($Ca_{10}(VO_4)_6(OH)_2$, isostructural to calcium hydroxyapatite) is a good catalyst in the formation of carbon-carbon bond reactions (Hara et al., 2006; Parhi, Upreti, & Ramanan, 2010). From the structural viewpoint, vanadium ions have various oxidation states and can adopt a variety of coordination geometries such as VO_4 tetrahedra, square VO_5 pyramids, or VO_6 octahedra, depending on the reaction conditions (Zavalij, & Whithingham, 1999). Among these, the tetrahedral VO_4 building unit is commonly observed and found to show very rich structural diversities and interesting properties with the secondary transition metals and organic species (Hagrman, Fin, & Zubieta, 2001).

We have been interested in the synthesis and structural chemistry of metal vanadium oxide-based compounds for a considerable amount of time (Chainok et al., 2010; Chanthee et al., 2012). As a continuation of our investigations, we report the successful synthesis of a new sodium vanadate

viz. $(Na_6F(H_2O)_{18})[(VO_4)_2]\cdot 2H_3O\cdot 2HF$ (**1**), which was prepared in high yield (up to 95%) by simply mixing the precursors V_2O_5 and NaOH in aqueous solution followed by the addition of a few drops of HF at room temperature. Single crystal X-ray diffraction analysis revealed that **1** is a discrete supramolecular aggregate organized via extensive hydrogen bonding networks. It was noted that although sodium vanadium oxides have been reported, for example, $Na_4(VO)_2(CF_3CO_2)_8(THF)_6(H_2O)_2$ (Cotton, Lewis, & Mott, 1983), $Na[V_6O_6F(OH)_3\{(OCH_2)_3CCH_3\}_3]\cdot 3H_2O$ (Khan et al., 1993), and $[NH_3(CH_2)_2(NH_2)(CH_2)_2NH_3]_3[\{Na(H_2O)\}\square\{V_4O_4F_2(O_3PCH_2PO_3)_4\}]\cdot 8H_2O$ (Smith et al., 2013), to the best of our knowledge, this is the first example of such vanadate oxide-based material comprising hexanuclear sodium $(Na_6F(H_2O)_{18})$ cluster. Moreover, the discrete structure of **1** can be transformed into an infinite three-dimensional (3D) sodium vanadate (β-$NaVO_3$) upon thermally induced solid-state reactivity**.**

2. Objectives

The aim of this work was to explore the new vanadate-based material containing sodium ion and to study its physical properties.

3. Materials and methods

All reagents were of analytical grade (≥98%), were purchased from commercial sources (TCI Chemicals), and were used without further purification. Elemental analysis was determined with a LECO CHNS 932 elemental analyzer. Powder X-ray diffraction (PXRD) measurements were carried out on a Bruker D8 ADVANCE X-ray powder diffractometer using Cu Kα (λ = 1.5418 Å). The simulated powder patterns were calculated from single crystal X-ray diffraction data and processed by the Mercury program version 2020.2.0 (Macrae et al., 2020). Infrared (IR) spectra were recorded in the ATR mode by using a Perkin-Elmer model Spectrum GX FTIR spectrometer in the range of 400–4000 cm^{-1}. Energy dispersive X-ray fluorescence spectrometer (EDXRF) responses was collected with an Orbis PC micro-XRF spectrometer equipped with a 50W Rhodium anode X-ray tube.

3.1 Synthesis of **1**

A mixture of V_2O_5 (36.4 mg, 0.2 mmol) and NaOH (4.0 mg, 0.1 mmol) was added to a 20 mL borosilicate glass vial containing distilled H_2O (5 mL) and the mixture was vigorously stirred (900 rpm) for 30 min at room temperature. Then five drops of 1M HF were added to the mixture under constant stirring (900 rpm) for 10 min. After filtration, colorless block-shaped single crystals of **1** were obtained in 95% yield, based on V_2O_5. Anal. Calcd for $H_{44}F_3Na_6O_{28}V_2$: H, 5.62%. Found: H, 5.47%. IR (ATR, ν/cm^{-1}, br for broad, m medium): 3231br, 1649m, 1390m, 980w, 751m.

Table 1 Crystal data and structure refinement for **1**

Compound	**1**
Empirical formula	$F_3H_{38}Na_6O_{26}V_2$
Formula weight	750.34
Temperature (K)	100(2)
Crystal System, Space group	Cubic**,** *Fd*-3*c*
a, *b*, *c* (Å)	28.034(3), 28.034(3), 28.034(3)
α, *β*, *λ* (°)	90, 90, 90
V (Å^3)	22033(8)
Z	32
D_{calc} (g/cm^3)	1.810
F(000)	12307
2*θ* range (°)	8.922 to 144.564
Radiation	Cu-Kα (λ = 1.54184 Å)
Reflection collected	33700
Independent reflections	921
R_{int}, R_{sigma}	0.0339, 0.0104
Data/restraints/parameters	921/36/108
Goodness-of-fit on F^2	1.188
Final *R* indexes [$I > 2\sigma(I)$]	R_1 = 0.0176, wR_2 = 0.0522
Final *R* indexes [all data]	R_1 = 0.0189, wR_2 = 0.0531
$\Delta\rho_{max}$, $\Delta\rho_{min}$ (e Å^{-3})	0.21, −0.38

3.2 X-ray crystallography

X-ray diffraction data of **1** were collected using a Bruker D8 VENTURE CMOS PHOTON 200 with graphite monochromated Cu-Kα (λ = 1.54184 Å) radiation at 100(2) K. Data reduction was performed using SAINT and SADABS scaling algorithm were used for absorption correction. The structure was solved with the ShelXT structure solution program using combined Patterson and dual-space recycling methods (Sheldrick, 2015a). The structure was refined by least squares using ShelXL (Sheldrick, 2015b). All non-H atoms were refined anisotropically. The H atoms attached to H_2O molecules and F ions were located in difference Fourier maps but refined with O−H = 0.82 ± 0.01 Å with U_{iso}(H) = 1.5U_{eq}(O) and F−H = 0.80 ± 0.01 Å with U_{iso}(H) = 1.5U_{eq}(F). While the oxonium molecules in **1** are highly disordered and could not be precisely modelled, thus the SQUEEZE subroutine of the PLATON program (Spek, 2003) was applied to remove residual electron density. A summary of crystal data for **1** is given in Table **1**. Crystallographic data for **1** have been deposited in the Cambridge Crystallographic Data Centre, CCDC numbers 2026135.

4. Results and discussion

4.1 Crystal structure

The single crystal X-ray diffraction analysis at 100(2) K revealed that **1** crystallizes in the highly symmetry cubic system of space group *Fd*-3*c*. There are two crystallographically unique V atoms and one unique Na atom in the asymmetric unit. The bond valence sum calculation (Brown, & Altermatt, 1985) indicates that the oxidation state of both V atoms is pentavalent and Na is monovalent. As can be seen in Figure 1a, the Na_6 hexameric core has a crystallographic center of inversion, and is composed of six Na^+ ions bridged *via* twelve corner-sharing μ_2-O atoms from water molecules, one F^- ion located in the middle of the core, and six H_2O molecules in the apical site. The Na^+ ions are all in similar six-coordinated octahedral [$NaFO_5$] geometries. The Na−O bond lengths fall in the range 2.3630(9) to 2.450(5) Å, which are typical values for the water-bridged sodium dimers (Shreeve et al., 2019). Simultaneously, the distorted octahedral F center lies about an inversion center, and is surrounded by six Na^+ atoms with the F−Na bond length of 2.4026(5) Å. It should be noted that there are very few examples of six-coordinated F centers (Wang, & Mak, 2000; Liu et al., 1994), none of which involves [FNa_6], thus, **1** is the first example of the octahedral F ion surrounded with six Na^+ atoms as proven via a search in the CSD ConQuest program version 2020.2.0 (Bruno, 2002). The packing diagram of the Na_6 hexameric cluster is depicted in Figure 1b. The nearest Na···Na separation between the hexameric core is about 6.15 Å.

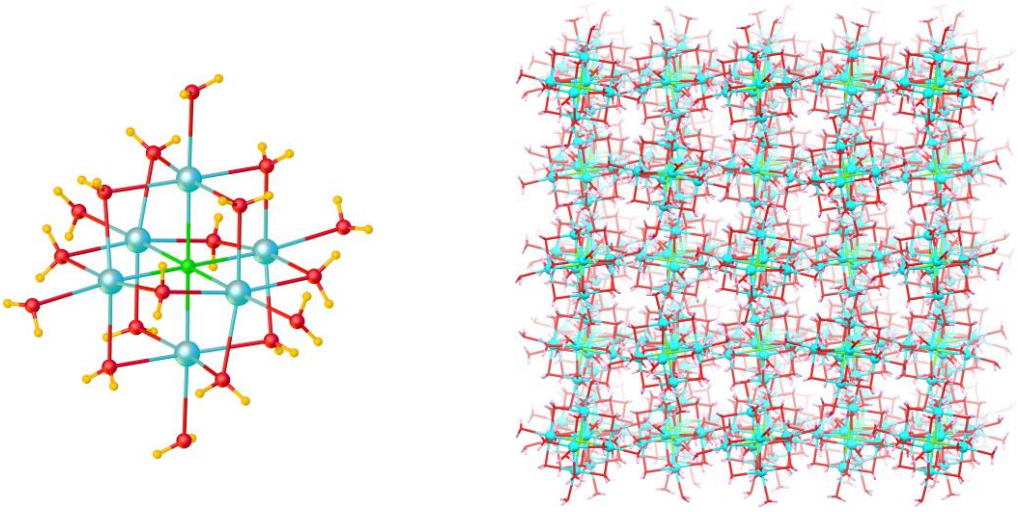

(a) (b)

Figure 1 Views of (a) the hexameric Na_6 core and (b) packing diagram of $[Na_6F(H_2O)_{18}]^{5+}$ cluster in **1** (the arctic, green, red, and yellow balls represent Na, F, O, and H atoms, respectively).

As shown in Figure 2a, the four-coordinated V1 atom locates on a two-fold rotation axis. Whereas, the V2 atom is on a three-fold rotation axis, and is found to be disordered over 3 sites with unequal occupancies. The V−O bond lengths are in the range of 1.694(7) to 1.7198(7) Å, which are comparable with those reported for other vanadate compounds (Chainok et al., 2011; Chanthee et al., 2012). The (VO_4) framework surface of **1** is also shown in Figure 2b. Apparently, extensive O−H···O hydrogen bonding networks are observed between the coordinated H_2O donor molecules and the terminal vanadyl sites of VO_4 units as well as the HF molecules as acceptor sites, Figures 2c,d. The O···O and O···F distances range from 2.290(8) to 3.079(2) Å. Additionally, the HF molecule behaves as a trifurcated hydrogen bond donor, participating in F–H···O interactions with the terminal oxygen atoms of (VO4) units with the F···O distances being 2.167(7) and 2.439(3) Å. Notably, the distances of these intermolecular O···O and O···F interactions are about 10−30% shorter than the sum of van der Waals radii of oxygen (1.52 Å) and fluorine (1.47 Å) (Bondi, 1964), indicating relatively strong intermolecular interactions. The geometrical details of hydrogen bonding interactions in **1** are listed in Table 2.

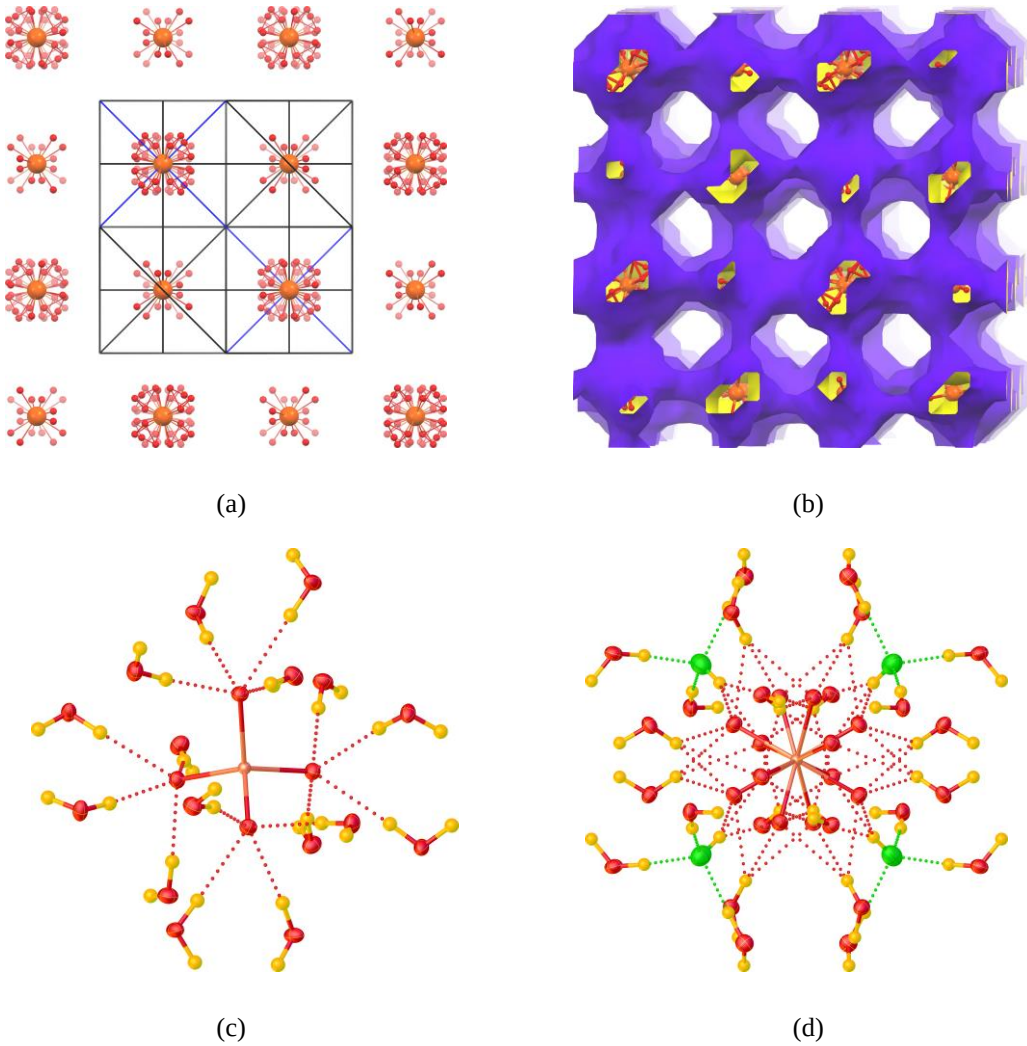

Figure 2 (a) Packing diagram of (VO_4) units (black and blue lines represent a 2-fold rotation axis and a 3-fold rotation axis, respectively) and (b) a view of the (VO_4) framework surface of **1**. Views of hydrogen bonding interaction (dashed lines) at (c) $V1O_4$ and (d) $V2O_4$ sites in **1**.

Table 2 Hydrogen-bond geometry (Å, °) for **1** at 100(2) K

D−H···*A*	*D*−H	H···*A*	*D*···*A*	*D*−H···*A*
F1−H1···O5*A*	0.75	1.74	2.439(3)	154
F1−H1···O5*A*[1]	0.75	1.74	2.439(3)	154
F1−H1···O5*A*[2]	0.75	1.74	2.439(3)	154
F1−H1···O5*B*	0.75	1.41	2.167(7)	180
O1−H1*A*···O5*A*	0.82(1)	2.13(2)	2.747(3)	133(2)
O1−H1*A*···O5*A*[3]	0.82(1)	2.15(1)	2.867(3)	146(2)
O1−H1*A*···O5*A*[4]	0.82(1)	1.99(1)	2.797(3)	173(2)
O1−H1*A*···O5*B*[5]	0.82(1)	2.30(1)	3.079(2)	161(2)
O1−H1*B*···O4[4]	0.83(1)	2.02(1)	2.823(3)	165(2)
O3−H3*A*···F2	0.81(2)	1.48(2)	2.290(8)	175(4)
O3−H3*B*···O4	0.82(2)	1.96(2)	2.785(6)	177(3)
O3*A*−H3*AA*···O3*A*[6]	0.79(2)	1.77(3)	2.442(1)	142(4)
O3*A*−H3*AB*···O4	0.83(2)	1.86(2)	2.688(7)	173(3)
O5−H5*A*···O4[6]	0.82(1)	2.03(1)	2.839(1)	175(2)
O5−H5*B*···O4[2]	0.82(1)	1.95(1)	2.767(1)	175(2)

Symmetry codes: (1) z, −x+5/4, −y+5/4; (2) −y+5/4, −z+5/4, x; (3) −z+3/4, −x+5/4, y−1/2; (4) −x+3/4, y, −z+3/4; (5) y−1/2, −z+5/4, −x+3/4; (6) −x+1, z+1/4, y−1/4.

4.2 Physical properties

PXRD analysis was conducted in order to confirm the phase purity of **1**. As shown in Figure 3a, the peak positions of the experimental PXRD patterns corroborate well the simulated ones derived from SC-XRD data, confirming good phase purity of the crystal samples. It should be noted that the reflection intensities of the simulated pattern are different from those of the experimental pattern due to the variation in preferred orientation of the crystalline samples during the PXRD experiments. The FT-IR spectrum of **1** is shown in Figure 3b. The broad absorption band in the region 3724−2504 cm^{-1} and at 1649 cm^{-1} are attributed to the O−H stretching and the O−H bending of coordinated H_2O molecules, respectively. The characteristic peaks at 980 and 751 cm^{-1} correspond to the V−O stretching of the orthovanadate anion (Li et al., 2018; Wang et al., 2018). Additionally, the EDXRF profile clearly shows the presence of vanadium element in the crystalline samples of **1**, Figure 3c. The results are consistent with the structure characteristics as determined by SC-XRD above. Furthermore, the thermal behavior of **1** was also investigated under a N_2 atmosphere in the temperature range of 30-1000 °C, and the result is provided in Figure 3d. The thermal decomposition of **1** displays rapid weight loss of 45.2% from 30 to 140 °C, which is probably due to the loss of water, oxonium and hydrofluoric acid molecules (calculated 50.9%). Upon further heating to 150 °C, a new phase was produced as seen from PXRD patterns (Figure 3a). Further heating up to 1000°C resulted in the formation of sodium metavanadate (β-$NaVO_3$: PDF 00-001-0246) (Kato, & Takayama, 1984).

5. Conclusion

In summary, a new sodium vanadate solid, namely, $(Na_6F(H_2O)_{18})[(VO_4)_2]\cdot 2H_3O\cdot 2HF$ (**1**) was successfully prepared using a simple and fast synthetic process with good yield (up to 90%) and high purity. The material **1** was characterized by means of SC-XRD, PXRD, FT-IR, TGA, and elemental analysis. To the best of our knowledge, this is the first example of a sodium vanadate solid built up from hexameric Na_6-comprising $(Na_6F(H_2O)_{18})^{5+}$ entities, and crystallized in highly symmetry cubic system with space group *Fd*-3*c*. **1** exhibits a discrete structure, where the four components (i.e. $(Na_6F(H_2O)_{18})$, (VO_4), H_3O and HF) are held into a 3D supramolecular architecture via extensive and strong O−H···O, O−H···F, and F−H···O hydrogen bonding interactions. Notably, the discrete structure of **1** can be transformed to a 3D network of sodium metavanadate (β-$NaVO_3$) phase via thermally induced solid-state reactivity upon slow heating to 1000 °C. In addition, **1** was completely soluble in water and some organic solvents such as acetone, methanol, ethanol, and acetonitrile. Finally, **1** possesses the well-defined hydrogen-bonding networks, which may play a vital role in fast proton transfer, implying a possible application in proton conductive materials.

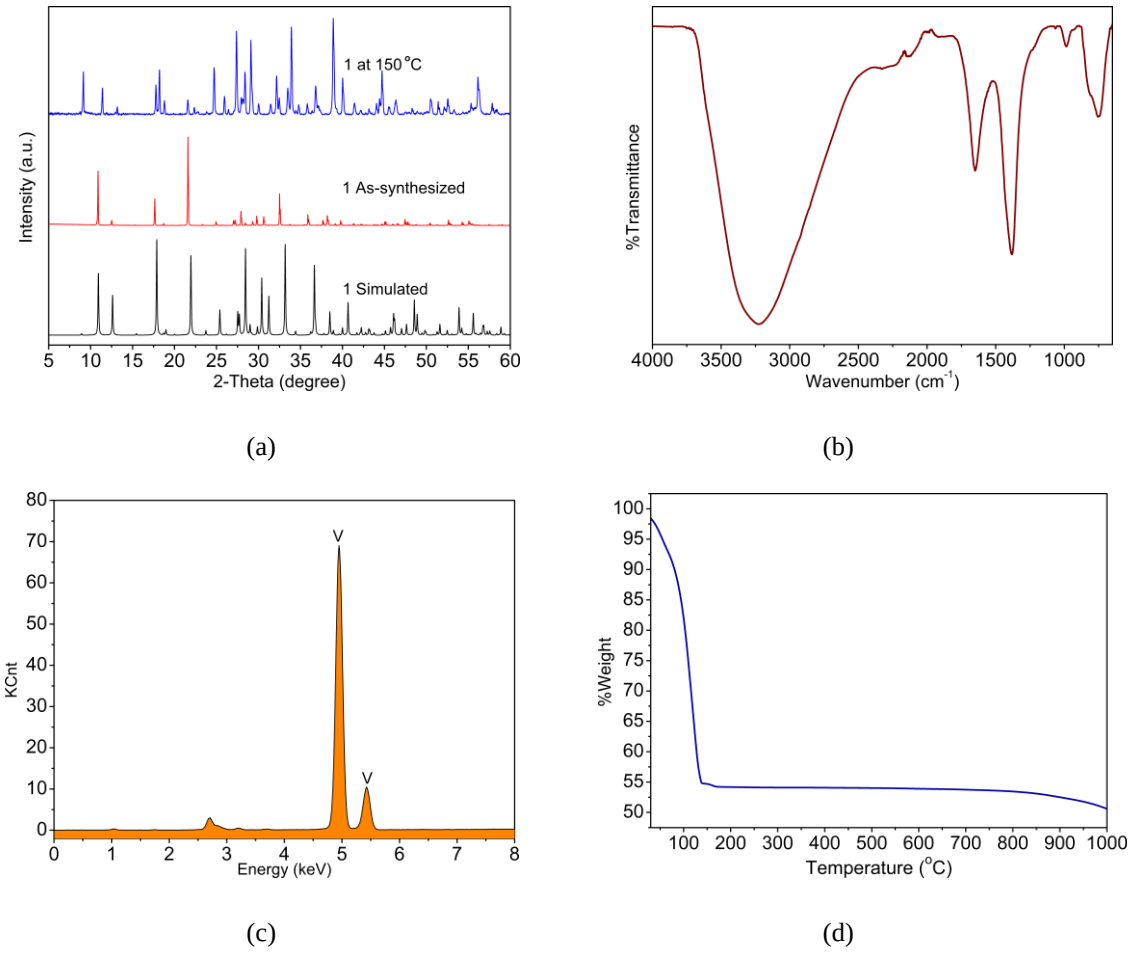

Figure 3 (a) PXRD patterns, (b) FT-IR spectrum, (c) EDXRF spectrum, and (d) TGA curve of **1**.

6. Acknowledgements

This work was supported by Thammasat University Research Unit in Multifunctional Crystalline Materials and Applications (TU-McMa). The authors thank the Faculty of Science and Technology, Thammasat University, for funds to purchase the single crystal X-ray diffractometer. C.P. acknowledges the Research and Researchers for Industries (RRI) funds (contact No. MSD62I0086) and Rangsit University for financial support.

7. References

Akande, A. A., Rammutla, K. E., Moyo, T., Osman, N. S. E., Nkosi, S. S., Jafta, C. J., & Mwakikunga, B. W. (2015). Magnetism variations and susceptibility hysteresis at the metal-insulator phase transition temperature of VO_2 in a composite film containing vanadium and tungsten oxides. *Journal of Magnetism and Magnetic Materials*, *375*, 1-9. DOI: 10.1016/J.JMMM.2014.08.099

Bondi, A. (1964). van der Waals Volumes and Radii. *The Journal of Physical Chemistry*, *68*(3), 441-451. DOI: 10.1021/j100785a001

Bouloux, J. C., Milosevic, I., & Galy, J. (1976). Magnesium hypovanadates $MgVO_3$ and MgV_2O_5. Crystal structure of $MgVO_3$. *Journal of Solid State Chemistry*, *16*(3-4), 393-398. DOI: 10.1016/0022-4596(76)90056-6

Brown, I. D., & Altermatt, D. (1985). Bond-valence parameters obtained from a systematic analysis of the Inorganic Crystal Structure Database. *Acta*

Crystallographica, *B41*, 244-247. DOI: 10.1107/S0108768185002063

Bruno, I. J., Cole, J. C., Edgington, P. R., Kessler, M., Macrae, C. F., McCabe, P., Pearson, J., & Taylor, B. (2002). New software for searching the Cambridge Structural Database and visualizing crystal structures. *Acta Crystallographica*, *B58*(Pt 3 Pt 1), 389-397. DOI: 10.1107/S0108768102003324

Chainok, K., Haller, K. J., Rae, A. D., Willis, A. C., & Williams, I. D. (2011). Investigation of the structure and phase transitions of the polymeric inorganic-organic hybrids: $[M(Im)_4V_2O_6]_\infty$; M = Mn, Co, Ni, Im = imidazole. *Acta Crystallographica*, *B67*(1), 41-52. DOI: 10.1107/S0108768110042941

Chanthee, S., Saesong, T., Saphu, W., Chainok, K. & Krachodnok, S. (2012). Poly[octakis-(1*H*-imidazole-κN^3)octa-μ-oxido-tetra-oxidodicopper(II)tetravanadate(V)]. *Acta Crystallographica*, *E68*, m362-m363. DOI: 10.1107/S1600536812008252

Cong, H., Zhang, H., Yao, B., Yu, W., Zhao, X., Wang, J., & Zhang, G. (2010). $ScVO_4$: Explorations of novel crystalline inorganic optical materials in rare-earth orthovanadate systems. *Crystal Growth & Design*, *10*(10), 4389-4400. DOI: 10.1021/CG1004962

Cotton, F. A., Lewis, G. E., & Mott, G. N. (1983). Dinuclear and polynuclear oxovanadium(IV) compounds. 2. A complicated sodium oxovanadium(IV) trifluoroacetate compound, $Na_4(VO)_2(CF_3CO_2)_8(THF)_6(H_2O)_2$. *Inorganic Chemistry*, *22*(12), 1825-1827. DOI: 10.1021/ic00154a027

Gopal, R., & Calvo, C. (1974). Crystal structure of magnesium divanadate, $Mg_2V_2O_7$. *Acta Crystallographica*, *B30*, 2491-2493. DOI: 10.1107/S0567740874007400

Hara, T., Kanai, S., Mori, K., Mizugaki, T., Ebitani, K., Jitsukawa, K., & Kaneda, K. (2006). Highly efficient C−C bond-forming reactions in aqueous media catalyzed by monomeric vanadate species in an apatite framework. *The Journal of Organic Chemistry*, *71*(19), 7455-7462. DOI: 10.1021/JO0614745

Khan, M. I., Chen, Q., Hope, H., Parkin, S., O'Connor, C. J. & Zubieta, J. (1993). Hydrothermal synthesis and characterization of hexavanadium polyoxo alkoxide anion clusters: crystal structures of the vanadium(IV) species $Ba[V_6O_7(OH)_3\{(OCH_2)_3CCH_3\}_3]\cdot 3H_2O$ and $Na_2[V_6O_7\{(OCH_2)_3CCH_2CH_3\}_4]$, of the mixed-valence complex $(Me_3NH)[V^{IV}_5V^{V}O_7(OH)_3\{(OCH_2)_3CCH_3\}_3]$, and of the fluoro derivative $Na[V_6O_6F(OH)_3\{(OCH_2)_3CCH_3\}_3]\cdot 3H_2O$. *Inorganic Chemistry*, *32*(13), 2929-2937. DOI: 10.1021/ic00065a022

Kato, K., & Takayama, E. (1984). Das Entwässerungsverhalten des Natriummetavanadatdihydrats und die Kristallstruktur des *β*-Natriummetavanadats. *Acta Crystallographica*, *B40*, 102-105. DOI: 10.1107/S0108768184001828

Li, S., Zhang, L., Lu, B., Yan, E., Wang, T., Li, L., Wang, J., Yu, Y., & Mu, Q. (2018). A new polyoxovanadate-based metal-organic framework: synthesis, structure and photo-/electro-catalytic properties. *New Journal of Chemistry*, *42*(9), 7247-7253. DOI: 10.1039/C7NJ05032A

Liu, F.-Q., Kuhn, A., Herbst-Irmer, R., Stalke, D. & Roesky, H. W. (1994). Molecular solids as ligands in organometallic chemistry: $[Cp_6{*}Ti_6Na_7F_{19}\cdot 2.5\ thf]$ (Cp* = C_5Me_5) and $[Cp_4{*}Ti_4Mg_2F_{12}\cdot 7thf]$, links between ionic solids and organometallic compounds. *Angewandte Chemie International Edition*, *33*(5), 555-556. DOI: 10.1002/ANIE.199405551

Macrae, C. P., Sovago, I., Cottrell, S. J., Galek, P. T. A., McCabe, P., Pidcock, E., Platings, M., Shields, G. P., Stevens, J. S., Towler, M., & Wood, P. A. (2020). Mercury 4.0: from visualization to analysis, design and prediction. *Journal of Applied Crystallography*, *53*, 226-235. DOI: 10.1107/S1600576719014092

Mattelaer, F., Geryl, K., Rampelberg, G., Dobbelaere, T., Dendooven, J., & Detavernier, C. (2016). Atomic layer deposition of vanadium oxides for thin-film lithium-ion battery applications. *RSC Advances*, *6*(115), 114658-114665. DOI: 10.1039/C6RA25742A

Millet, P., Satto, C., Sciau, P. & Galy, J. (1998). MgV_2O_5 and $\delta Li_xV_2O_5$: a comparative structural investigation. *Journal of Solid State Chemistry*, *136*(1), 56-62. DOI: 10.1006/jssc.1997.7654

Parhi, P., Upreti, S., & Ramanan, A. (2010). Crystallization of calcium vanadate solids from solution: a metathetic route. *Crystal Growth & Design*, *10*(12), 5078-5084. DOI: 10.1021/CG100703H

Shanmugam, M., Ayyaru, S., & Ahn, Y. (2018). Enhanced cathode performance of rGO-V_2O_5 nanocomposite catalyst for microbial fuel cell application. *Dalton Transactions*, *47*, 16777-16788. DOI: 10.1039/C8DT02445F

Sheldrick, G. M. (2015*a*). SHELXT − Integrated space-group and crystal-structure determination. *Acta Crystallographica Section A: Foundations and Advances*, *71*(Pt 1), 3-8. DOI: 10.1107/S2053273314026370

Sheldrick, G. M. (2015*b*). Crystal structure refinement with SHELXL. *Acta Crystallographica*, *C71*, 3-8. DOI: 10.1107/S2053229614024218

Shreeve, J., Zhang, J., Zhang, J., Imler, G., & Parrish, D. (2019). Sodium and potassium 3,5-dinitro-4-hydropyrazolate: three-dimensional metal–organic frameworks as promising super-heat-resistant explosives. *ACS Applied Energy Materials*, *2*(10), 7628-7634. DOI: 10.1021/acsaem.9b01608

Smith, T. M., Mahne, N., Prosvirin, A., Dunbar, K. R., & Zubieta J. (2013). A tetranuclear oxofluorovanadium(IV) cluster encapsulating a $Na(H_2O)_{n+}$ subunit. *Inorganic Chemistry Communications*, *33*, 1-5. DOI: 10.1016/j.inoche.2013.03.027

Spek, A. L. (2003). Single-crystal structure validation with the program PLATON. *Journal of Applied Crystallography*, *36*(Pt 1), 7-13. DOI: 10.1107/S0021889802022112

Wang, K., Xu, Q., Ma, P., Zhang, C., Niu, J., & Wang, J. (2018). Polyoxovanadate catalysts for oxidation of 1-phenyl ethanol: from the discrete $[V_4O_{12}]^{4-}$ and $[V_{10}O_{28}]^{6-}$ anions, to the anionic $[V_6O_{17}]_n^{4n-}$ coordination polymer. *CrystEngComm*, *20*, 6273-6279. DOI: 10.1039/C8CE01237G

Wang, O.-M. & Mak, T. C. W. (2000). Novel layer-type triple salts of silver(I), $AgCN{\cdot}AgF{\cdot}4AgCF_3CO_2{\cdot}2L$ (L = MeCN or H_2O) Dedicated to the memory of Professor George Alan Jeffrey (1915-2000). *Chemical Communications*, 1435-1436. DOI: 10.1039/B003821K

Wanna, W. H., Janmanchi, D., Thiyagarajan, N., Ramu, R., Tsai, Y.-F., Pao, C.-W., & Yu, S. S.-F. (2019). Selective catalytic oxidation of benzene to phenol by vanadium oxide nanorod (Vnr) catalyst in CH_3CN using H_2O_2(aq) and pyrazine-2-carboxylic acid (PCA). *New Journal of Chemistry*, *43*, 17819-17830. DOI: 10.1039/C9NJ02514F

Zavalij, P. Y. & Whittingham, M. S. (1999). Structural chemistry of vanadium oxides with open frameworks. *Acta Crystallographica*, *B55*(Pt 5), 627-663. DOI: 10.1107/S0108768199004000